



Printability of calcium phosphate powders for three-dimensional printing of tissue engineering scaffolds

Andre Butscher^{a,b,*}, Marc Bohner^a, Christian Roth^c, Annika Ernstberger^a, Roman Heuberger^a, Nicola Doebelin^a, Philipp Rudolf von Rohr^c, Ralph Müller^b

^aRMS Foundation, Bischmattstrasse 12, CH-2544 Bettlach, Switzerland

^bInstitute for Biomechanics, ETH Zurich, Wolfgang-Pauli-Strasse 10, CH-8093 Zurich, Switzerland

^cInstitute of Process Engineering, ETH Zurich, Sonneggstrasse 3, CH-8092 Zurich, Switzerland

ARTICLE INFO

Article history:

Received 26 June 2011

Received in revised form 12 August 2011

Accepted 31 August 2011

Available online 6 September 2011

Keywords:

Three-dimensional printing (3DP)

Tissue engineering

Calcium phosphates (CaP)

Powder flowability

Powder wettability

ABSTRACT

Three-dimensional printing (3DP) is a versatile method to produce scaffolds for tissue engineering. In 3DP the solid is created by the reaction of a liquid selectively sprayed onto a powder bed. Despite the importance of the powder properties, there has to date been a relatively poor understanding of the relation between the powder properties and the printing outcome. This article aims at improving this understanding by looking at the link between key powder parameters (particle size, flowability, roughness, wettability) and printing accuracy. These powder parameters are determined as key factors with a predictive value for the final 3DP outcome. Promising results can be expected for mean particle size in the range of 20–35 μm , compaction rate in the range of 1.3–1.4, flowability in the range of 5–7 and powder bed surface roughness of 10–25 μm . Finally, possible steps and strategies in pushing the physical limits concerning improved quality in 3DP are addressed and discussed.

© 2011 Acta Materialia Inc. Published by Elsevier Ltd. All rights reserved.

1. Introduction

A paradigm shift is taking place in medicine from using synthetic implants and tissue grafts to a tissue engineering approach that uses degradable porous material scaffolds integrated with biological cells or molecules to regenerate tissues [1]. Tissue engineering is commonly defined as an interdisciplinary field that applies the principles of engineering and life sciences toward the development of biological substitutes that restore, maintain or improve tissue function or a whole organ [2]. The standard approach in bone tissue engineering is based on scaffolds seeded and cultivated with bone cells *in vitro* or *in vivo*. Scaffolds typically consist of highly porous three-dimensional (3-D) structures that aim at temporarily mimicking the natural extracellular matrix of bone. In this sense scaffold engineering sets high demands on design and material.

From a material point of view, timing between resorption and tissue growth rate is critical for the choice of an adequate material. In that respect, calcium phosphate (CaP) ceramics are promising candidates because they have a long history and are widely used in synthetic bone replacement due to their chemical similarity with bone minerals [3,4]. More importantly, some calcium phos-

phates, such as β -tricalcium phosphate (β -TCP; $\text{Ca}_3(\text{PO}_4)_2$), are known to provide a smooth transition between a bone defect and mature bone [5].

From a design point of view conventional production techniques fail to meet the high demands of highly porous and interconnected porous networks for cell growth, flow transport of nutrients and metabolic waste [6]. Therefore layer-based solid free-form fabrication, also referred as rapid prototyping, is a serious alternative [1]. Three-dimensional printing (3DP) is a versatile solid free-form technique characterized by a high flexibility in material and geometry [7]. A broad range of powdered materials can be synthesized by 3DP to simple solid or complex-shaped scaffolds. Powder-based 3DP is also capable of generating well-defined open porous cellular solids out of bioactive calcium phosphate powder [8–11]. Using calcium phosphate powders local solidification can be achieved by ejecting a liquid (binder) out of a printhead onto the powder. In this case binding results from the formation of crystals between the powder particles. More details on 3DP can be found in a recently published review article [7].

One of the drawbacks of 3DP is its relatively limited spatial resolution, typically close to 0.1–0.2 mm [12,13]. Also, as printed scaffolds lay in a powder bed and as it is difficult to remove powders from small cavities, porous scaffolds can only be printed with pores larger than ~ 0.5 mm [14–17]. Unfortunately, this value is at the upper limit of the pore sizes that are supposed to be adequate for tissue engineering [18]. Therefore, there is a great need to

* Corresponding author at: RMS Foundation, Bischmattstrasse 12, CH-2544 Bettlach, Switzerland. Tel.: +41 32 644 1400; fax: +41 32 644 1176.

E-mail address: Andre.Butscher@rms-foundation.ch (A. Butscher).

improve printing resolution and accuracy in order to produce more relevant scaffold architectures. There are several process factors limiting the 3DP accuracy. There are printing system factors such as positioning and resolution of the printhead as well as its smallest binder drop size. The binder drop size is highly critical due to its ballistic impact on the powder bed. Powder bed stability is defined in this paper as the capacity of the powder bed to withstand ballistic impact or deposition of a new powder layer. However, printhead technology in most cases is a black box for applied 3DP research in the area of tissue engineering. Therefore focusing on powder and binder solution properties is reasonable. One approach to reach higher accuracy is to improve the powder properties. Unfortunately, the relation between the initial powder properties and the final quality of printed scaffolds is poorly understood [7]. In the literature, suggestions for particle size minima can be found between 10 and 50 μm in order to overcome critical spreading issues of dry powder particles [12,19,20]. Particles are also suggested to be less than 40 μm in order to obtain acceptable resolution, while resolution is at least twice the powder size [19]. However these suggestions are just rough guidelines. They do not take into consideration the particle morphology and surface roughness (affecting the flowability) or the surface free energy (affecting the wettability with the binder solution), both crucial factors for 3DP. Therefore this study aims at better understanding the interplay between powder properties and 3DP printability. In printing and thick film technology [21–23], the term printability generally refers to rheology and thixotropy (shear-stress-dependent viscosity) of suspensions or gels. In this paper printability is defined by powder characteristics essential for the 3DP process such as reactivity, flowability and wettability. This paper focuses on the flowability and wettability as basic preconditions for powder-based 3DP.

Flowability of powdered material is an essential parameter for the layer-based additive process of 3DP. High flowability of adequate powders allows the roller to build up thin layers (recoating) and thus high 3DP resolution. A too low flowability reduces the printing resolution due to insufficient recoating. A too high flowability does not provide a powder bed stability large enough for 3DP. Another crucial factor for 3DP is the wettability of the powder bed particles by the binder solution. The amount of binder solution absorbed and the volume distributed within the powder bed determines resolution (voxel size) and mechanical properties (strength of chemical bonding). However, the wetting mechanism of a powder by binder droplets is very complex [24]. A too low wetting of fine powder particles can result in powder bed rearrangement possibly detrimental for further 3DP [25]. A too high wetting and slow powder reaction will reduce the smallest feature size.

The above-mentioned principles suggest that a relation between powder properties and the final 3DP scaffold properties must exist. However, there is a lack of knowledge in this relation, partly due to limited methods to determine powder flowability and wettability. In spite of the given theoretical and technical limitations, this study aims at a better understanding of the interplay between relevant powder properties and printability for currently available methods. This allows systematic comparison of powders and sets a foundation for further improvement in 3DP for scaffold engineering applications.

2. Material and methods

2.1. Powders

Five custom-made β -tricalcium phosphate (β -TCP, $\beta\text{-Ca}_3(\text{PO}_4)_2$) powders (Medicoat AG, CH) were used in this study (Table 1). These powders had different particle size distributions (small (S), medium (M), large (L), extra large (XL), and extra-extra large

(XXL)). Moreover, a part of the smallest fraction was plasma-treated (S_{plasma}) to enhance its flowability (see details hereafter). Additionally, two control powders were included in this study. The first one (ZP 130, Z Corporation, Burlington, MA, USA) is sold by the company manufacturing the 3-D printer used in this work. The second powder is an α -TCP produced according to a procedure described in detail in Ref. [26]. The only differences are the use of a lower Ca/P ratio (1.45) and slightly higher sintering temperatures (1400 °C). This α -TCP powder is more reactive than β -TCP, but availability and cost justify the use of β -TCP as the main test material.

A 0.45:1 M ratio blend of calcium carbonate powder (CC, CaCO_3 ; Merck, Germany, Art. No. 102076) and dicalcium phosphate powder (DCP, CaHPO_4 ; GFS Chemical, USA, Art. No. 1548) was mixed end-over-end for 1 h using a Turbula mixer (Bachofen, Switzerland). It was then calcined at 900 °C for 1 h in an LHT 02/16 furnace (Nabertherm, Germany), cooled to room temperature and ground in a mortar with a pestle until all could pass through a 0.125 mm sieve. The calcined and sieved blend was then placed on calcium stabilized ZrO_2 plates (S-3406, Zircoa, USA), sintered at 1400 °C for 4 h and then removed from the furnace to quench the powder in air. The sintered powder was then broken in a jaw crusher (BB51, Retsch, Germany), milled and sieved to get the desired particle range.

The plasma treatment was conducted in a plasma downstream reactor according to a patented procedure [27] described in detail in the literature [28–30]. In this process the flowability can be enhanced by plasma-enhanced chemical vapour deposition of SiO_x nanoparticles on the surface of the substrate powder. The nanoparticles emerge from the monomer hexamethyldisiloxane (HMDSO) and act as spacers between the substrate powder particles, thus increasing the distance between their surfaces and reducing the predominant van der Waals forces [31].

2.2. Powder characterizations

Various characterizations techniques were applied on the tested powders, including X-ray photoelectron spectroscopy (XPS) to determine the surface composition of plasma-coated particles, laser diffractometry to determine the particle size distribution (PSD) of the powders, scanning electron microscopy (SEM) to visualize particle morphology, X-ray diffraction (XRD) to check the crystalline composition, nitrogen adsorption to quantify the specific surface area (SSA) of the powders, a ring-shear tester and custom-made funnels to determine the powder flowability, and finally a tensiometer to measure powder wettability. Details of these various techniques are given hereafter.

2.2.1. X-ray photoelectron spectroscopy

The amount of SiO_x nanoparticle deposition on the surface of the substrate TCP powder was investigated using XPS analysis (Axis NOVA, Kratos Analytical, Manchester, UK). The photoelectrons were excited using monochromatic $\text{AlK}\alpha$ radiation with a power of 225 W (15 kV, 15 mA); an area of $700 \times 300 \mu\text{m}^2$ was analysed. The analyser ran in the fixed-analyser-transmission mode with a pass energy of 40 eV for the detailed and 80 eV for the survey spectra (full width at half-maximum for $\text{Ag } 3d_{5/2} = 0.6$ and 0.9 eV, respectively) at a take-off angle of 90°. The residual pressure was below 1×10^{-6} Pa. The system was calibrated according to ISO 15472:2010 with an accuracy of ± 0.05 eV or better.

The data processing was performed using CasaXPS software (V2.3.15, Casa Software Ltd., UK). Charging of the sample was corrected by referencing aliphatic carbon to 285.0 eV [32]. Prior to the peak fitting an iterated Shirley background was subtracted [33]. For the calculation of the quantitative composition the peak areas

Table 1Percentiles of particle size distribution ($d_{10}/d_{50}/d_{90}$), specific surface area (SSA), bulk and tapped densities, and compaction (ratio of bulk and tapped densities).

Powder	$d_{10}/d_{50}/d_{90}$ (μm)	SSA ($\text{m}^2 \text{g}^{-1}$)	ρ_{Bulk} (kg m^{-3})	ρ_{Tapped} (kg m^{-3})	$\rho_{\text{Tapped}}/\rho_{\text{Bulk}}$ (-)
S	2/7/14	1.01 ± 0.01	662 ± 13	1299 ± 22	1.96
S _{Plasma}	2/7/14	1.01 ± 0.01	955 ± 8	1505 ± 5	1.58
M	11/18/28	0.34 ± 0.02	1055 ± 2	1440 ± 3	1.36
L	16/27/39	0.30 ± 0.02	1108 ± 7	1428 ± 3	1.29
XL	15/35/54	0.32 ± 0.01	1061 ± 1	1346 ± 14	1.27
XXL	20/51/75	0.29 ± 0.01	1065 ± 4	1297 ± 6	1.22
ZP 130	8/32/79	0.62 ± 0.02	1169 ± 2	1579 ± 6	1.35

were corrected by the transmission function and the sensitivity factors given by Kratos assuming a homogeneous compound.

2.2.2. Particle size distribution

The particle size distribution of the dry powder was measured by laser diffraction (Helos & Rodos, Sympatec, Germany). For this purpose the powder was reproducibly dispersed by a vibratory chute feeding the powder into an air stream prior to laser diffraction measurement.

2.2.3. Scanning electron microscopy

Scanning electron microscopy (Zeiss EVO MA 25, Zeiss, Germany) was used to assess the particle morphology of the different powder fractions. The samples were sputtered (SCD 050 Sputter Coater, Baltec, Switzerland) with a thin layer of gold (~ 10 nm, sputter time 40 s at 40 mA) and carbon (two-ply carbon yarn, 8×10^{-6} mbar vacuum). For high resolution (magnification of 40,000) SEM pictures, the samples were only sputtered with a very thin gold layer (~ 7 nm, 25 s at 40 mA).

2.2.4. X-ray diffraction

X-ray diffraction patterns were measured on a Philips PW1800 diffractometer with graphite-monochromated $\text{CuK}\alpha 1$ radiation in the range $4\text{--}60^\circ 2\theta$. The quantitative phase composition was determined by Rietveld refinement using the software FullProf.2k version 4.40 [34]. Structural models were taken from Dickens et al. [35] for β -TCP, Sudarsanan and Young [36] for hydroxyapatite, Boudin et al. [37] for β -calcium pyrophosphate and Mathew et al. [38] for α -TCP. No other phases were identified in the diffraction patterns. Crystallite sizes of the main phases were calculated from isotropic peak broadening using the Scherrer equation [39]. Since the different β -TCP powder fractions were all produced from the same raw material, X-ray diffraction data were determined for samples of the powder fractions S, S_{Plasma}, M, XL only. Additionally for comparison reasons XRD patterns were also recorded for the ZP 130 and α -TCP powder samples.

2.2.5. Specific surface area

The SSA was determined by nitrogen adsorption (Gemini 2360, Micromeritics, USA), applying the Brunauer Emmet Teller (BET) equations. The TCP powders were dried at 130°C for 3 h in order to remove moisture residuals prior to the SSA characterization. The ZP 130 powder was heated up to a temperature of 100°C only, due to thermal decomposition at approximately 130°C .

2.2.6. Bulks and tapped density

Bulk and tapped densities were determined according to standardized test methods [40,41]. While for the bulk density a given powder volume was weighed without tapping, the powder specimen for the tapped density was first tapped with 150 taps and then weighed.

2.2.7. Flowability

2.2.7.1. Ring shear tester. According to Schulze [42] powder flowability can be reproducibly measured with a ring shear tester (RST-XS, Schulze Schüttgutmesstechnik, Germany).

The ring shear cell was filled with a volume of 30 ml powder, the pre-shear stress was set to 1500 Pa, and shear stresses of 300/750/1200/300 N were applied. The measurement was repeated three times for each sample. Flowability was expressed by the so-called flow factor (ff_c). According to Ref. [43], ff_c is defined as the ratio of the consolidation stress σ_1 and the compression strength σ_c :

$$ff_c = \frac{\sigma_1}{\sigma_c}$$

Schulze proposed the following classification as a measure for the following qualitative flowability ranges: $ff_c > 10$: free flowing, $4 < ff_c < 10$: easy flowing, $2 < ff_c < 4$: cohesive, $1 < ff_c < 2$: very cohesive, $ff_c < 1$: non-flowing.

2.2.7.2. Custom-made glass funnel method. A simple alternative based on funnels was used to assess flowability. For that purpose, glass funnels (diameter: 46 mm, angle: 35°) with different orifices (diameter of 8/12/18/24/30/36 mm) were filled in a reproducible manner and lifted up by hand (Fig. 1). If the powder flew out, the procedure was repeated with the next smaller diameter. The outcome was a simple but reliable pass/nonpass powder ranking for different cylinder orifices.

2.2.8. Wettability

Wettability of the powder was quantified by measuring the contact angle between the fluid/gas and the fluid/solid interface. As the powder surface was not dense and smooth, the contact angle between the baseline of the drop and the tangent at the drop boundary had to be measured dynamically, using a high speed camera and an automated drop positioning system. An attempt was made to use the Drop Shape Analysis DSA 100 (Krüss, Germany) but unfortunately this method delivered irreproducible results. Specifically, positioning of small binder drops was difficult. Additionally the reproducibility of the powder bulk and surface preparation was poor and highly impacted the results. Therefore this approach was replaced by the more robust capillary penetration method described in detail in the literature [24,44]. A schematic illustration of this method can be found in Fig. 2 [45]. Each powder was filled and compacted in a glass cylinder with a permeable bottom. The capillary force is mainly determined by the void dimensions between the particles and their surface properties. The measurements were performed with a Tensiometer K100 (Krüss, Germany). The contact angle Θ was derived from the Washburn equation [46,47]:

$$\frac{m^2}{t} = \frac{c \cdot \rho_L^2 \cdot \sigma_L \cos \Theta}{\eta_L}$$

where m is the mass of absorbed liquid, t the absorption time, c the capillary constant, ρ_L the liquid density, σ_L , the surface tension of

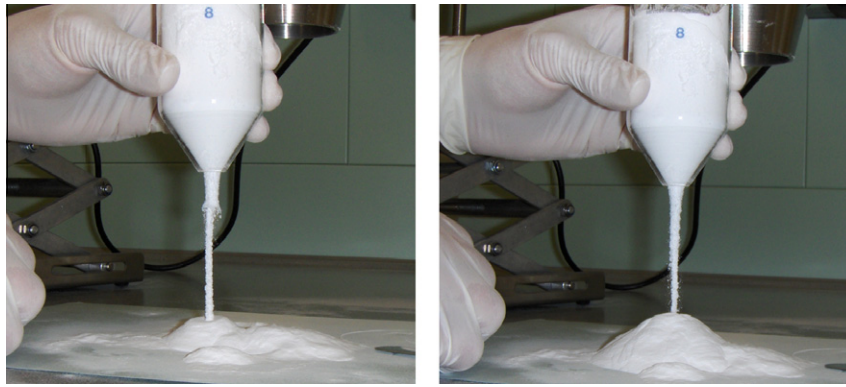


Fig. 1. Custom-made glass funnels with different orifices (here diameter 8 mm) used for simple glass funnel flowability measurement.

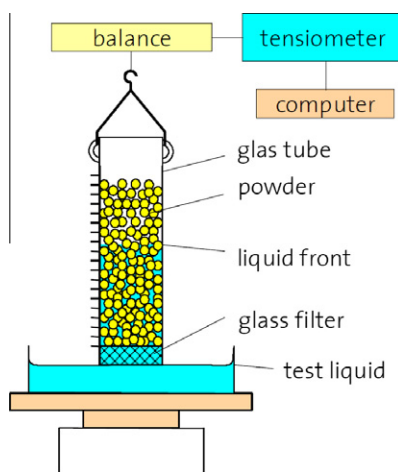


Fig. 2. Schematic illustration of the contact angle measurement according to Washburn (with permission by Dr. C. Arpagaus).

the liquid, and finally η_L the dynamic viscosity of the liquid. The penetration rate (m^2/t) is determined by linear regression in the linear part after initial wetting and before the fluid reaches the top of the wetted powder specimen. The capillary constant c was determined in a pre-test using a perfectly wetting liquid (*n*-hexane with a contact angle of nearly $\Theta = 0^\circ$ ($\cos\Theta = 1$), Fluka No. 52770). Since this constant depends on the powder and its degree of compaction, it was determined for each investigated powder. Furthermore, powder compaction was performed in a reproducible manner described in detail in [Supplementary data](#).

Ideally, the contact angle measurements should be performed with the liquid used for 3DP. But since the 10 wt.% phosphoric acid solution would react with the tested powder, a 0.2 M Na_2HPO_4 solution was used for the wetting experiments. More details concerning the wettability measurement can be found in the [Supplementary data](#).

2.3. 3-D printer

A commercial 3-D printer (Zprinter 310plus, Z Corporation, Burlington, USA) was used in this study. However, custom-made feed and build reservoirs were installed to reduce the build volume to $\sim 10\%$ of the ZCorp original setup to allow 3DP with smaller powder amounts. Printing parameters were adjusted to a layer thickness of 88 μm and a binder/volume ratio of 0.28 for the shell and 0.14 for the core of the 3DP part. Printing parameters were chosen according to the literature [48] and kept constant for all printing tests.

After printhead (HP 10 black printhead, C4800A, ink drop size 35 pl according to HP) purging with water, diluted 10 wt.% phosphoric acid was used as a binder solution. Phosphoric acid solution partially dissolves the calcium phosphate powder, subsequently leading to precipitation of new calcium phosphate crystals bridging the powder particles together.

3-D models were generated with the CAD software NX 7.5 and imported to the 3-D printing software in the “.stl” (stereolithography) file format. In this study a pyramid geometry (step size 2 mm, overall length/width/height 20 mm) was used for comparison of 3DP of the different powder fractions.

2.4. Powder bed and scaffold characterizations

2.4.1. Roughness of the powder bed

Surface roughness analysis of 3-D printed parts can be found in the literature [49]. In this study the roughness of the powder bed prior to binder deposition was quantified with a new method described in more details in [Supplementary data](#). In summary, the 3-D printer was used to staple five powder layers, and the resulting bed surface was photographed from two different angles using SEM. A surface reconstruction algorithm was then applied to quantify the surface roughness.

2.4.2. Characterization of the printed scaffolds

For all the powder fractions, pyramid structures were printed if feasible three times, cleaned with compressed air and finally photographed in a reproducible manner. This procedure served to qualitatively assess the 3DP outcome, taking into account the whole 3DP process chain. Since the quality of the printed parts differed drastically with a change of raw materials, no further characterization was performed.

2.5. Statistics

Statistical analysis was done using a two-way ANOVA and student *t*-test.

3. Results

In [Fig. 3](#) an overview and a close up of the particle morphology of every powder class are presented. The SEM images show that the β -TCP particles have an irregular shape, with mostly sharp edges. Whereas the largest particle fractions consist of single particles, the smallest fraction seems to consist of agglomerates. Nevertheless, the PSD ([Fig. 4](#)) of the β -TCP powders was monomodal. The PSD of the small particles was broader than that of the other powders. The SEM photos also showed a clear variation of the

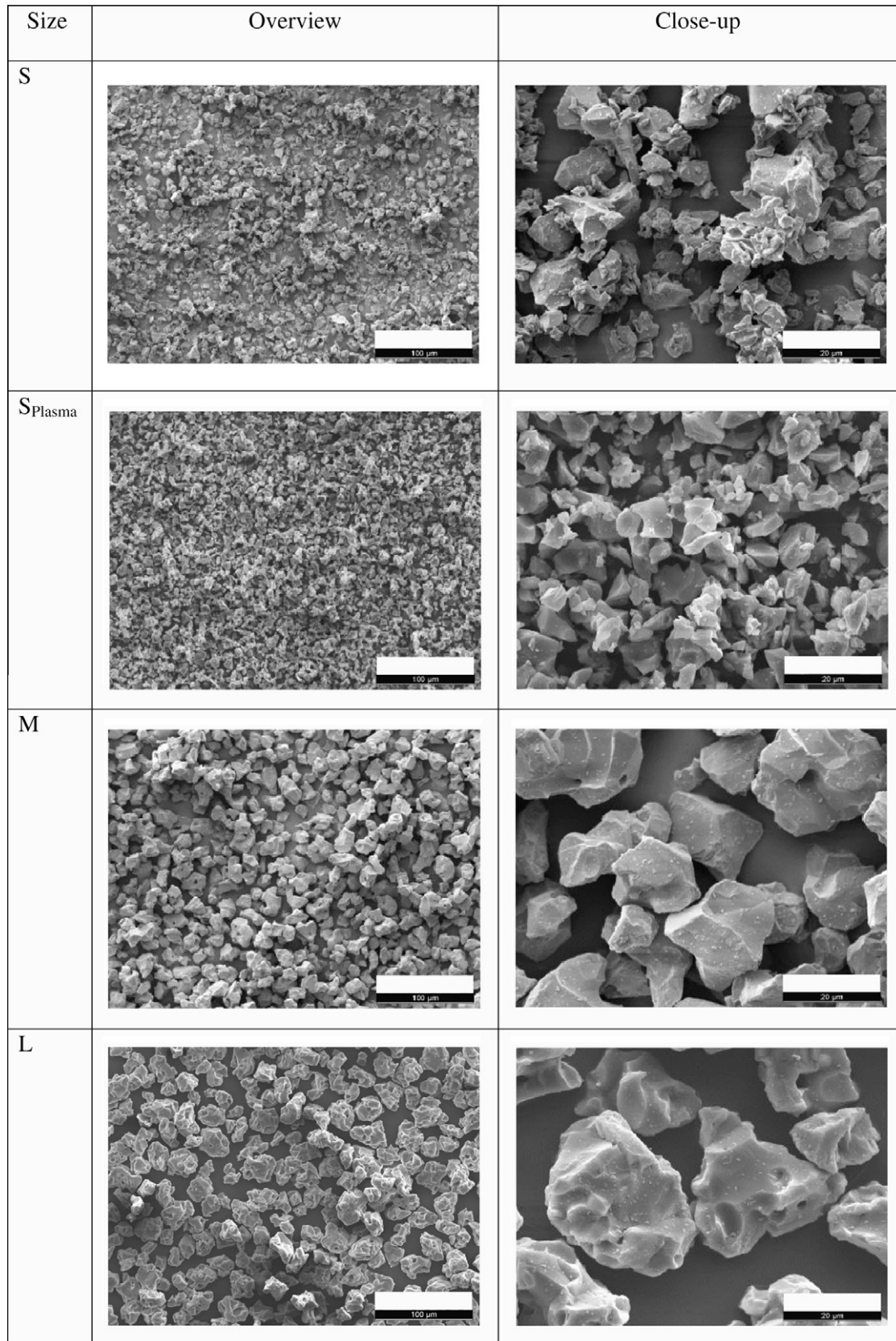


Fig. 3. Particle size and morphology of different powder fractions overview (left, 100 μm bar) and close up (right, 20 μm bar).

particle size between the various β -TCP powders, in agreement with the particle size distribution measurements. The ZP 130 powder contained hexagonal prisms and a broad PSD. The mean parti-

cle sizes of the β -TCP powders determined by laser diffractometry were in the range of $6.6 \pm 0.1 \mu\text{m}$ (S) to $50.7 \pm 0.1 \mu\text{m}$ (XXL). The value for the XL fraction ($35.13 \pm 0.04 \mu\text{m}$) was close to the mean

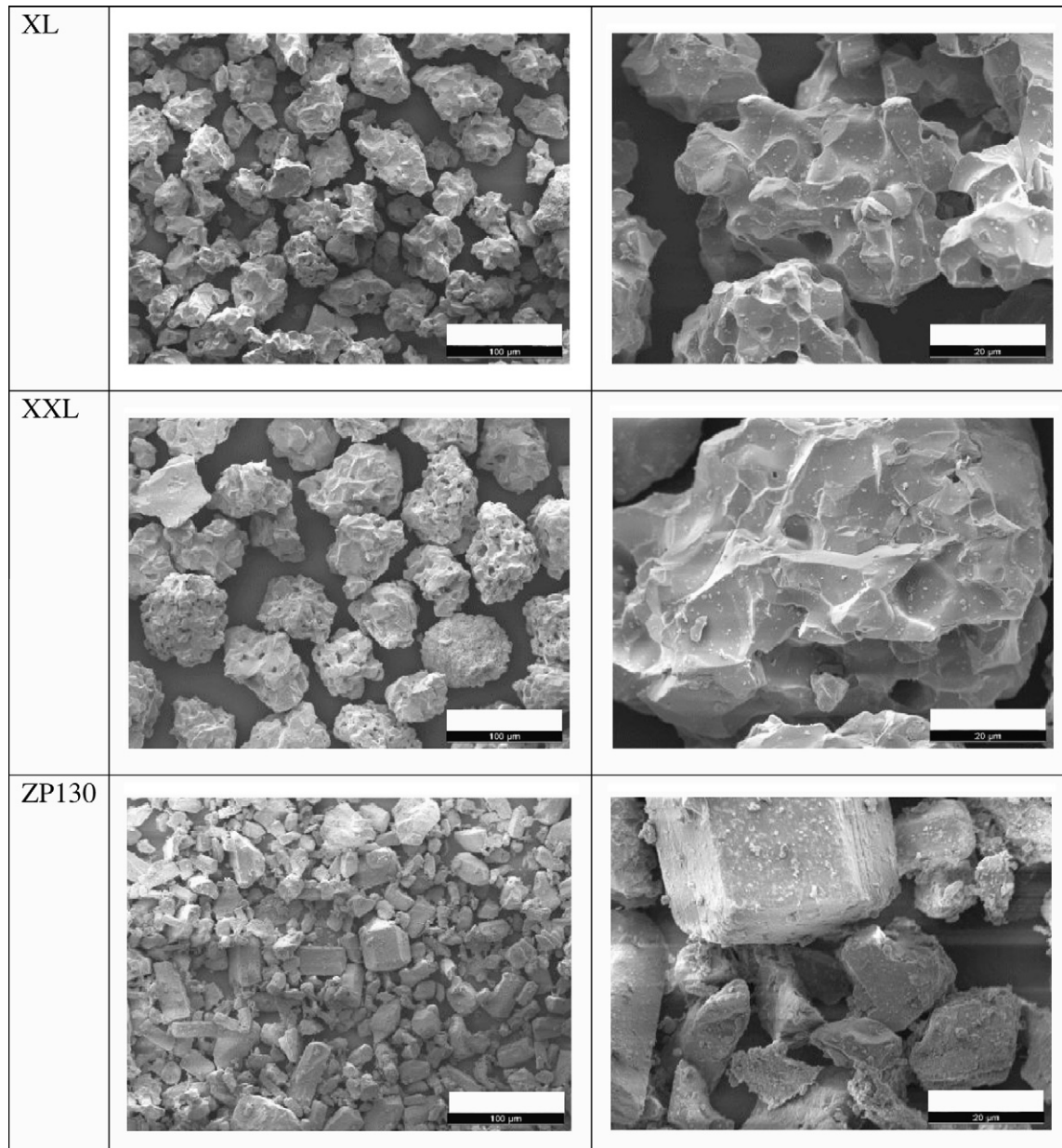


Fig. 3 (continued)

particle size of the ZP 130 powder ($31.9 \pm 0.2 \mu\text{m}$). Detailed results of the density distributions of the different powder fractions are summarized in Table 1. Fractions are classified according to their median particle size d_{50} of $8 \mu\text{m}$ (S), $6 \mu\text{m}$ (S_{plasma}), $18 \mu\text{m}$ (M), $29 \mu\text{m}$ (L), $40 \mu\text{m}$ (XL) and $40 \mu\text{m}$ (XXL). Further characterizations of the different powders are summarized in Table 1. Besides the powder size, SSA and bulk/tapped densities are presented.

The XRD measurement revealed a high β -TCP phase quantity (>95%) as well as small amounts of HA (<1%) and β -CPP (4%). The α -TCP sample was highly pure (99%), despite the fact that a nominal Ca/P ratio of 1.45 was selected to achieve higher sinterability. The ZP 130 consisted mostly of calcium sulfate hemihydrate (CSH, $\text{CaSO}_4 \cdot 0.5\text{H}_2\text{O}$) as well as small amounts of calcium sulfate anhydrate (CSA; CaSO_4). Crystallite sizes were determined in the range of 110–155 nm and 45–65 nm for β -TCP and α -TCP respectively. The α -TCP revealed about three times smaller crystallite size, leading to even higher reactivity and improved crystallization rate.

The XPS analysis revealed further insights in the chemical composition of the plasma deposited nanostructures. Fig. 5 shows the survey and detailed spectra of plasma-treated and untreated powder with prominent signals of oxygen, calcium, carbon, phosphorus and silicon. The binding energies of calcium, phosphorus and oxygen (Table 2) were as expected for a calcium phosphate compound [50]. On the untreated powder, a Si2p signal was found at 102.6 eV, which corresponded to silicates or silicones [50]. On the plasma-treated powder, the Si2p signal was with 103.3 eV at a much higher binding energy. Similar binding energies were found for plasma generated SiO_xC_y compounds [51]. Carbon was due to organic contamination on the sample and in the case of the plasma-treated powder partially due to carbon incorporated into the SiO_xC_y coating. The ratio of calcium to phosphorus was $1.4 \pm 0.1:1$, which is close to the theoretical ratio of 1.5 for β -TCP ($\beta\text{-Ca}_3(\text{PO}_4)_2$).

The interplay between particle size, flowability and roughness of the β -TCP powder fractions are graphically illustrated in Fig. 6. These results revealed a linear correlation ($R^2 = 0.96$) between

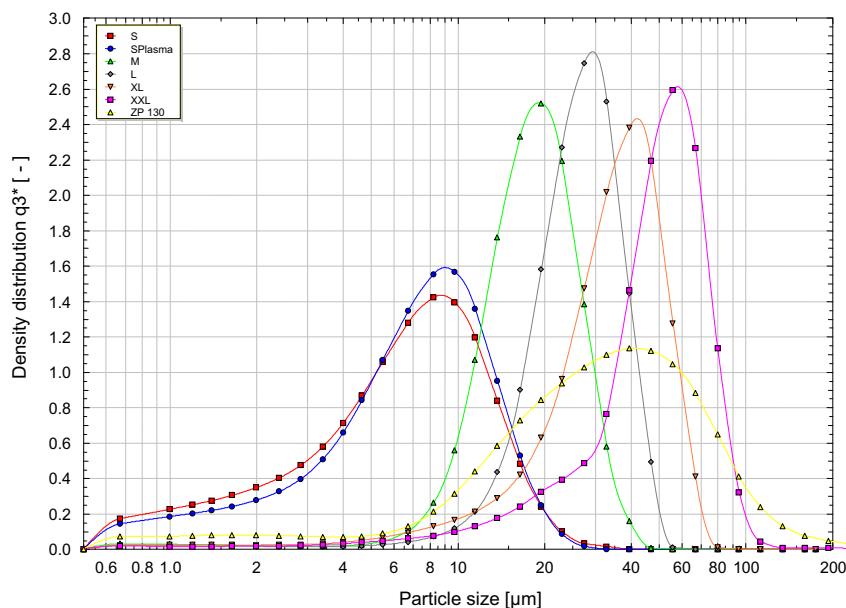


Fig. 4. Particle size distributions of β -TCP fractions S, S_{plasma} , M, L, XL, XXL and reference powder ZP 130.

the median particle size (d_{50}) and flowability. The statistical model detected significant differences between the different ff_c values ($p < 0.05$).

Qualitative results of printed surface roughness analysis can be found in Supplementary data (Fig. S2) while quantitative results are depicted in Fig. 7. No correlation ($R^2 < 0.1$) was found for the surface roughness. The statistical model revealed significant differences for the overall dataset ($p < 0.05$). Comparison of the M fraction to all other fractions resulted in significant differences ($p < 0.05$).

Contact angle measurement results with 0.2 M Na_2HPO_4 are depicted in Fig. 8. For this setup and specimen used in this investigation the contact angle values were small (good wettability) for large particles and large (poor wettability) for small particles. For the plasma-coated powder, no phosphate solution could be sucked up, suggesting a contact angle $>90^\circ$. As a result, it was not possible to determine the contact angle according to Washburn. A similar outcome was noticed with the ZP 130 powder due to immediate hydraulic reaction.

Quantitative results of flowability, surface roughness and contact angle measurements are summarized in Table 3.

Printing tests (Fig. 9; the complete results are presented in Supplementary Fig. S3) revealed that 3DP was not feasible with particles either too small (S) or too large (XXL) – not feasible in the sense that the pyramid steps were either distorted (XXL) or partially not built at all (S).

For fractions S and S_{plasma} , printing was stopped after one trial due to unacceptable powder bed recoating. For comparison the same pyramids were also printed with the standard ZCorp powder ZP 130 with the ZCorp binder Zb 58 as well as custom-made α -TCP powder with the same 10 wt.% phosphoric binder solution as used for the β -TCP fractions.

4. Discussion

The goal of this study was to relate powder properties and printability in a 3DP printer. For that purpose, a systematic approach was used where powders of the same composition (β -TCP) but different particle size distributions were used for 3-D printing. In all tests, the same binder solution (10 wt.% phosphoric

acid) and printing parameters were used. For simplicity the saturation was kept constant for all powders. It is believed that this is justified since the bulk density varied in a small range except for the S fraction (Table 1). However, the poor printing adequacy of the fraction S was not due to a lack of binding but rather an issue of flowability.

To assess the quality of the printed parts, two control groups were used; one consisting of samples produced with the commercial standard ZCorp powder ZP 130 and one consisting of samples produced with home made α -TCP powder.

SSA results (Table 1) show relatively constant outcome except for the S fractions (approximately three times higher) and the ZP 130 powder (approximately two times higher). High specific surface is beneficial due to higher reactivity with the binder solution. In this regard, the small powder fraction is superior to the other powder fractions. However, for successful 3DP, flowability and wettability needs to be taken into account. Small particles tend to agglomerate, which can also be identified on the SEM pictures (Fig. 3). In fine and dry powders, the attractive interactions between particles are mainly determined by van der Waals forces [31], which are proportional to the particle size for two spheres of equal size. For very fine or porous particles these forces can even dominate gravitational forces and thus dramatically reduce flowability. Therefore particle size and density are critical flowability factors. Additionally, irregular shapes of single and agglomerated particles induce poor flowability [52].

Flowability properties are difficult to estimate experimentally [53] despite their importance in early civilization times, for example for the storage of large quantities of bulk goods [54]. As a result, flowability analysis is still a matter of current research [29,55,56]. The term flowability summarizes all information about the ability of a bulk solid to flow under loads and arrange itself in its static state [53]. In other words, particles are assumed to behave like a fluid and are modelled as a homogenous continuum. However, this analogy has limitations. For example, when a vertical pressure is applied to a Newtonian fluid, the stresses are the same at every single point of the continuum and in all directions. In contrast, resulting horizontal stresses for a powder are lower than vertical stresses, with typical values for this relation in the range of 0.3–0.6 [57]. Therefore, any conclusion drawn from fluid mechanics might deceive and therefore this aspect needs special attention.

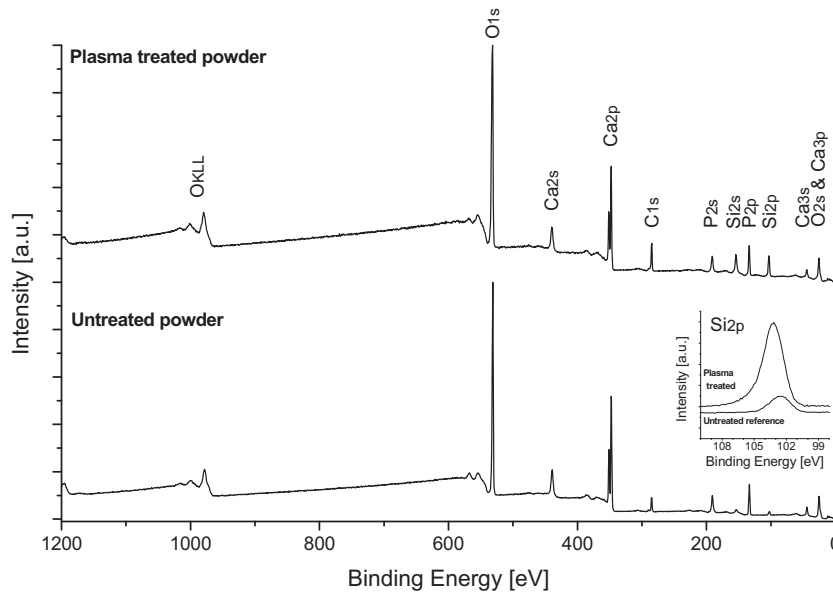


Fig. 5. XPS survey and detailed spectra of plasma-treated and untreated powder.

Table 2
Binding energies and atomic ratios (normalized by phosphorus) of the untreated and plasma-treated powder according to the XPS analysis.

	Atomic ratio (normalized by phosphorus)					
	Ca _{2p3/2}	P _{2p3/2}	Si _{2p}	Si _{2p}	O _{1s}	C _{1s}
Binding energies (eV)	347.7	133.4	102.6	103.3	531.5	285.0
Untreated sample	1.4	1.0	0.2		4.7	0.9
Plasma-treated sample	1.3	1.0		1.1	6.2	1.7

The accuracy of the binding energies is ±0.1 eV.

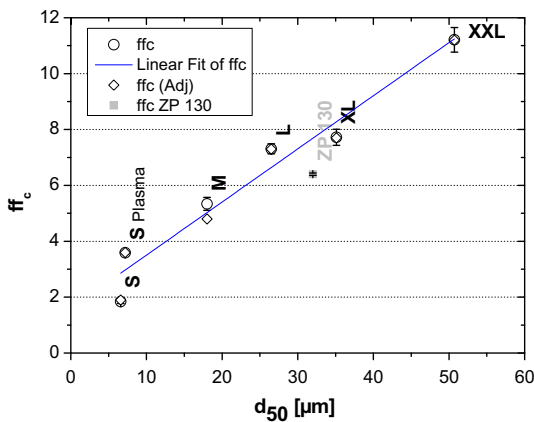


Fig. 6. Dependency of flowability (ff_c) on median particle size. The symbols (○) correspond to the mean values and the error bars to the standard deviation. The linear fit is based on the ff_c values of S, S_{Plasma}, M, L and XXL. The diamonds (◇) correspond to the adjusted values according to the statistical model.

This fact is especially critical taking into account that the vertical stresses vary in every powder specimen, even for non-compacted specimens due to gravitational forces. Therefore, reproducible measurement of powder flowability is facilitated by systematic compaction prior to testing.

Flowability is usually measured with simple funnel methods. Two approaches are widespread. First, in ISO 6186 [58] the time is recorded for a certain amount of powder to exit a well-defined

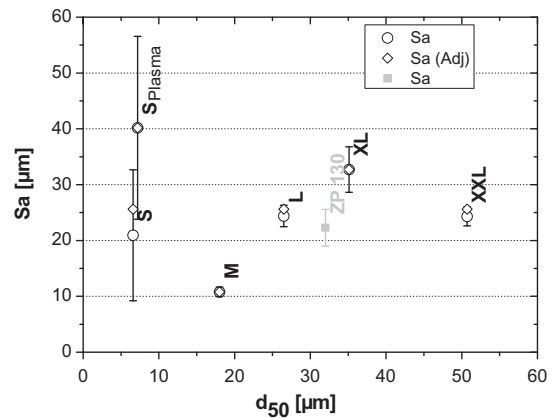


Fig. 7. Dependency of surface roughness (S_a) on median particle size. The symbols (○) correspond to the mean values and the error bars to the standard deviation. The diamonds (◇) correspond to the adjusted values according to the statistical model.

funnel. Second, in ISO 4324 [59] the angle of repose is calculated by height measurement of a powder pyramid, where low angles indicate a high flowability. However, these methods can be applied to powders with easy flowing characteristics only. Especially for the powder sizes used in 3DP, these methods have major limitations and reproducibility is not optimal. Therefore a custom-made funnel method was adapted and used to serve as a first and simple indicator for the flowability and thus feasibility for 3DP. A more sophisticated method according to Schulze [43] allows very reproducible powder flowability measurement. According to the results of this study (Table 3), ff_c values between 5 and 7 (reference powder ZP 130: 6.4 ± 0.04) seem to be optimal. While smaller values inhibit proper recoating, larger values result in powder bed instability. When comparing ff_c values with compaction results the following interesting relationship can be found for the powder size range relevant for 3DP: large compaction (relation of tapped over bulk density) seem to indicate poor flowability and vice versa (Table 1), because the powder compacts already more under the influence of gravity only if the flowability is high and the interparticle forces are low. During recoating the new powder bed is also compacted to a certain degree. This compaction mechanism taking

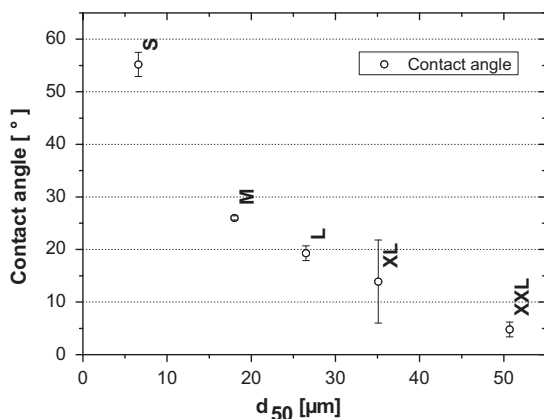


Fig. 8. Dependency of contact angle (with 0.2 M Na_2HPO_4 as wetting liquid) on median particle size (β -TCP powder fractions). The error bars correspond to the standard deviation.

Table 3

Flowability ff_c and funnel ranking, surface roughness S_a , contact angle α (values after \pm indicate standard deviation).

Powder	ff_c	Funnel (mm)	S_a (μm)	α ($^\circ$)
S	1.84 ± 0.07	36	40.2 ± 16.4	55.2 ± 2.3
S_{Plasma}	3.59 ± 0.03	8	20.9 ± 11.7	$>90^\circ$
M	5.34 ± 0.23	30	10.8 ± 0.9	26.0 ± 0.4
L	7.31 ± 0.18	30	24.4 ± 1.9	19.3 ± 1.4
XL	7.72 ± 0.29	24	32.7 ± 4.1	13.9 ± 7.9
XXL	11.21 ± 0.44	8	24.3 ± 1.7	4.8 ± 1.4
ZP 130	6.44 ± 0.04	36	22.3 ± 3.3	–

place while distributing and compacting a new layer with the counter rotating roller and its influence on flowability is not trivial [60]. The amount of compaction during 3DP will be higher than during bulk and lower than during tapped density measurement. Therefore measurement of both density values provides valuable predictive information concerning flowability and compaction rate for 3DP.

High powder flowability only is not sufficient for 3DP. Large powder particles (XXL, $d_{50} = 51 \mu\text{m}$) exhibit a very high flowability ($ff_c = 11.2$). However, 3DP of pyramids (Fig. 9) with XXL powder demonstrates layer displacements due to low powder bed stability and thus inadequate outcome. Additionally resulting powder bed surface with such large particles results in low accuracy since the largest particles determine minimal layer thickness and resolution. Resolution is generally at least twice the dimension of the particle size [19] while minimal layer thickness of at least three particles is suggested to facilitate powder flow [61]. Last but not least, post-printing depowdering with large particles and high surface roughness is very difficult and often not feasible. Minimum cavity diameter of five times the average powder size [62] is recommended for simple cavities while for complex cavities and structures this value should be higher. Therefore small particles are mandatory for high resolution. However, small particles typically exhibit low flowability and high surface roughness. On the other hand, a smooth surface quality of the top powder surface is required for 3DP [63]. Powder bed surface roughness (Table 3) exhibits a minimum in the range of the M powder. It can therefore be concluded that powders providing a surface roughness in the range of 10–30 μm (reference powder ZP 130: 22.3 μm) are adequate. Minimized powder bed surface roughness does not, however, imply minimized final surface roughness of 3DP solids. Another crucial requirement for 3DP is the wettability of the powder bed by the binder solution. Powder wetting depends on many parameters, such as the contact angle between binder solution and powder, the

binder solution viscosity, the topography of the powder bed surface (depending on particle shape and size) and the chemical reactions occurring between binder solution and powder [67]. In more detail microscopic and macroscopic contact angles need to be analysed separately [64]. Microscopic contact angle is independent of the surface geometry. It only depends on the physical properties of the liquid phase of the binder drop, the solid phase of the substrate and the surrounding air phase. However, the contact angle is typically not measured locally on a microscopic but on a macroscopic scale, which in our case is consisting of many powder particles. So, the measurement is made referencing a macroscopic surface tangent consisting of mountains and valleys, and gaps between particles are filled with air. This observation reveals the crucial importance of powder bed roughness and binder drop size in 3DP, determining whether micro- or macroscopic effects will dominate the wetting behaviour [64,65]. Taking into account the ballistic impact of binder drops with powder bed particles makes this task even more complex.

According to the present study the Washburn method is currently the only method enabling the assessment of wettability with reasonable empiric effort. Applying this method confirmed the relation that exists between particle size and contact angle; however, an optimal contact angle range could not be determined due to several limitations. The Washburn method is inadequate for hydrophobic particles with a contact angle of 90° and above. Furthermore, tests could not be made with the binder solution because of the reaction occurring between the binder solution and the powder. Therefore direct wetting quantification of the powder binder solution combination used in 3DP was not feasible and substitutions for the binder solution needed to be found. Additionally, dynamic impact of binder drops in the picoliter range with high speed on a dry powder bed seems very difficult to analyse and understand. Typically, binder drops with a diameter of tens of micrometers impinge at a speed $\sim 10 \text{ m s}^{-1}$ on a loosely laid-out powder bed, resulting in powder bed deformation and powder ejection highly affecting the quality of the final printed parts [66]. It is speculated that printhead technology allowing small binder drops in the order of a few picoliters will open new possibilities and challenges for high resolution in 3DP. Since the droplet powder interaction is a key factor within 3DP, this will be a challenging goal for future studies. Until now the only way to try to understand this process is to observe empirically the 3DP process and determine the final integrity of the printed specimen. The use of small binder droplet will allow the use of small powder particles and hence open the way to lower layer thickness and better depowdering characteristics. Until now the small particle approach was limited due to agglomeration tendency. This effect can, however, be reduced with a plasma coating.

XPS and SEM results indicate the feasibility of plasma surface modification of CaP powder particle surfaces. While the uncoated powder surface apart from larger CaP particles exhibits a relatively smooth surface, the plasma-coated surface shows a surface roughness induced by tiny point-like plasma depositions (Fig. 10). This point-like morphology of the deposited nanostructures is of high importance since they act as spacer between the powder particles. Due to the increase in the interparticle distance the attractive van der Waals forces are reduced and the flowability of dry powder in the micrometer range is improved [55]. Even though the plasma treatment induces also a reduction of the surface free energy, the main effect of flowability improvement is attributed to the created additional surface roughness as shown in a previous study [28]. In this way during our investigations, it was possible for the first time to build up smooth powder layers with the powder S_{Plasma} . However, wettability and powder bed stability of these powder layers were poor (Fig. 11). XPS analysis revealed that the binding energy of the Si2p signal increased from 102.6 to 103.3 eV. This shows that

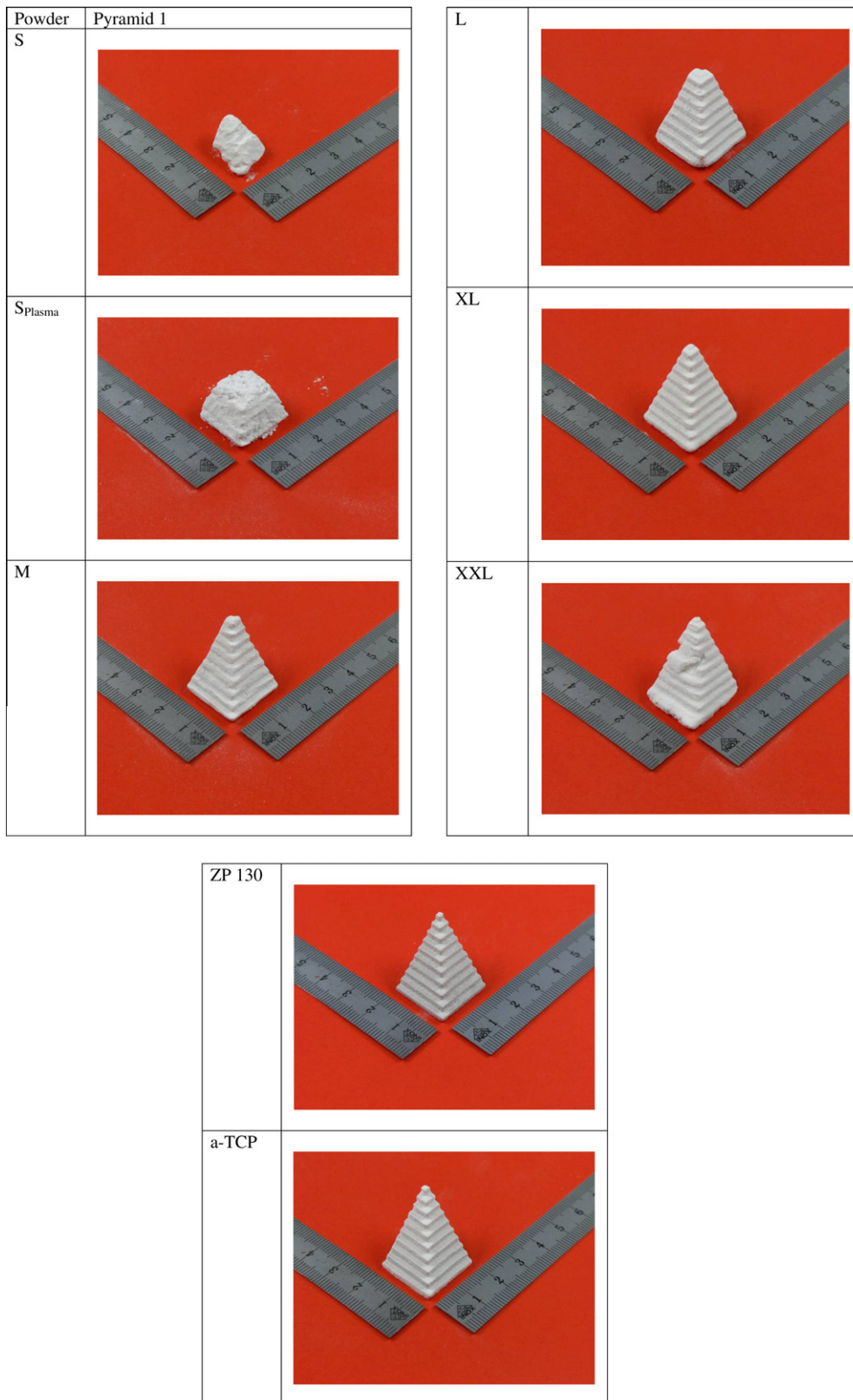


Fig. 9. Three-dimensional printing (3DP) of pyramids using different powder fractions.

the powder was previously contaminated by silicones or silicates and that with the plasma treatment, a SiO_xC_y compound was formed on the surface. For a plasma coating of flat polymeric sub-

strates produced with an O_2 :HMDSO ratio of 5:1, Korner et al. [51] found the Si2p peak at a binding energy of 103.4 eV, which correlated to a $\text{Si:O}_{1.6}:\text{C}_{0.4}$ compound. Since that binding energy was

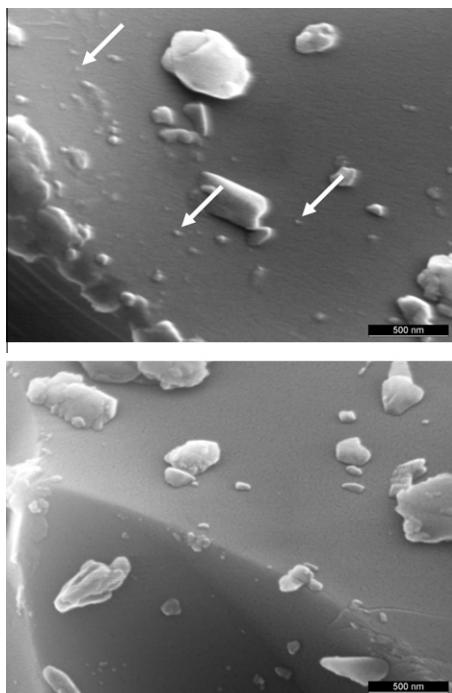


Fig. 10. Powder specimen S_{Plasma} (above) and S (below).

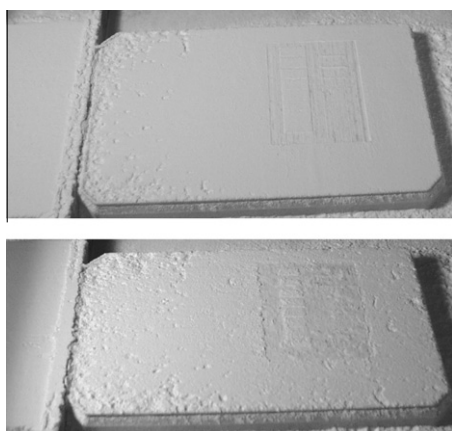


Fig. 11. Plasma-coated powder S_{Plasma} bed with (upper) and without (lower) moisture application prior to 3DP.

0.1 eV higher, the estimated ratio of the atomic composition for this study is roughly $\text{Si}:\text{O}_{1.5}:\text{C}_{0.5}$, which means that each silicon atom was bound to three oxygen atoms and one carbon atom. The carbon content in these structures might be an explanation for the hydrophobic characteristics of the plasma-treated powder. In our investigation, an $\text{O}_2:\text{HMDSO}$ ratio of ~ 10 was used. According to Ref. [51] an increase of this ratio to 30:1 results in a nearly pure SiO_2 compound, indicating an improvement in hydrophilic behaviour. This might be a reasonable step for future studies aiming at flowability and wettability optimization of CaP powder.

A strategy to enhance wettability during 3DP and overcome powder bed damage due to ballistic impact of binder solution in a small powder particle bed has been proposed earlier [67]. Specifically, spraying the powder bed surface with water vapour stabilizes the top layer surface and allows particle rearrangement and wetting instead of particle ejection out of the powder bed. The effect of the powder bed stabilization with the powder S_{Plasma} is illustrated in Fig. 11 (upper) and might open new approaches for high resolution powder-based 3DP.

A relatively simple way to account for the interplay of all the powder parameters is 3DP of simple structures such as pyramids illustrated in Fig. 9. Since the focus of this study was on powder parameters the outcomes of the printing were compared only qualitatively. The pyramids of the different powder fractions showed clear differences. While 3DP was not feasible for the smallest fractions S/S_{Plasma} (critical wetting and powder bed stability) and largest fractions XXL (critical layer displacement), fractions M, L and XL resulted in reasonable outcome. Resolution of the M powder was very promising and comparable to the standard powder ZP 130. However, mechanical integrity was so weak that even depowdering was very challenging. Therefore 3DP was repeated with α -TCP powder having similar morphological powder characteristics. The 3DP outcome of this α -TCP fraction revealed optimal results concerning mechanical integrity and geometrical accuracy. In the literature α -TCP is described as reactive alternative to β -TCP [26,68]. Only a few studies using α -TCP for 3DP printing have been published [69,70] probably because of availability and cost. Due to its higher reactivity, α -TCP might also be an interesting alternative with respect to the mechanical properties of 3DP constructs, which is still a matter of current and future research [71–73].

5. Conclusion and outlook

In conclusion, this investigation quantifies the 3DP relevant powder characteristics which in turn set a basis for systematic optimization. Promising results can be expected for mean particle size in the range of 20–35 μm , compaction rate $\rho_{\text{Tapped}}/\rho_{\text{Bulk}}$ in the range of 1.3–1.4, flowability ff_c in the range of 5–7 and powder bed surface roughness S_a of 10–25 μm .

The insights discussed allow preprint selection of powders, especially relevant for highly pure and costly powders for scaffold engineering. A prestudy with α -TCP showed very promising results concerning precision and geometrical accuracy (Fig. 9, α -TCP).

In powder-based 3DP, minimum feature size depends on the powder particle size and the binder drop size. While printhead technology is advancing towards smaller binder drops, handling of fine powders suitable for 3DP is very challenging. A promising way to tailor the wettability and flowability of fine powders for 3DP is plasma deposition. 3DP is a relatively young technique; with as high the obstacles currently seem, as great the chances are and will be.

Acknowledgements

Funding from RMS Foundation is gratefully acknowledged. The authors express their appreciation to Dr A. Spillmann from the Institute of Process Engineering for support with the plasma coating. W. Hirsiger, F. Bigolin and O. Loeffel from the RMS Foundation are acknowledged for SEM analysis. L. Galea from the RMS Foundation is acknowledged for support in statistical analysis. J. Lemaître from the EPFL in Lausanne (Switzerland) is acknowledged for his software used in this study to perform statistical analysis.

Appendix A. Supplementary data

Supplementary data associated with this article can be found, in the online version, at doi:10.1016/j.actbio.2011.08.027.

Appendix B. Figures with essential colour discrimination

Certain figures in this article, particularly Figures 1, 2, 4, 6 and 9, are difficult to interpret in black and white. The full colour images can be found in the on-line version, at doi:10.1016/j.actbio.2011.08.027.

References

- [1] Hollister SJ. Porous scaffold design for tissue engineering. *Nat Mater* 2005;4(7):518–24.
- [2] Langer R, Vacanti JP. Tissue engineering. *Science* 1993;260(5110):920–6.
- [3] Constantz BR, Ison IC, Fulmer MT, Poser RD, Smith ST, VanWagoner M, et al. Skeletal repair by in situ formation of the mineral phase of bone. *Science* 1995;267(5205):1796–9.
- [4] Dorozhkin SV, Epple M. Biological and medical significance of calcium phosphates. *Angew Chem Int Ed* 2002;41(17):3130–46.
- [5] Renooij W, Hoogendoorn HA, Visser WJ, Lentferink RHF, Schmitz MGJ, Vanieperen H, et al. Bioresorption of ceramic strontium-85-labeled calcium-phosphate implants in dog femora – a pilot-study to quantitate bioresorption of ceramic implants of hydroxyapatite and tricalcium ortho-phosphate invivo. *Clin Orthop Rel Res* 1985(197):272–85.
- [6] Hutmacher DW. Scaffolds in tissue engineering bone and cartilage. *Biomaterials* 2000;21(24):2529–43.
- [7] Butscher A, Bohner M, Hofmann S, Gauckler L, Muller R. Structural and material approaches to bone tissue engineering in powder-based three-dimensional printing. *Acta Biomater* 2011;7(3):907–20.
- [8] Maier AK, Dezmirean L, Will J, Greil P. Three-dimensional printing of flash-setting calcium aluminate cement. *J Mater Sci* 2011;46(9):2947–54.
- [9] Shanjani Y, De Croos JNA, Pilliar RM, Kandel RA, Toyserkani E. Solid freeform fabrication and characterization of porous calcium polyphosphate structures for tissue engineering purposes. *J Biomed Mater Res Part B* 2010;93B(2):510–9.
- [10] Klammert U, Reuther T, Jahn C, Kraski B, Kubler AC, Gbureck U. Cytocompatibility of brushite and monetite cell culture scaffolds made by three-dimensional powder printing. *Acta Biomater* 2009;5(2):727–34.
- [11] Warnke PH, Seitz H, Warnke F, Becker ST, Sivananthan S, Sherry E, et al. Ceramic scaffolds produced by computer-assisted 3D printing and sintering: characterization and biocompatibility investigations. *J Biomed Mater Res Part B* 2010;93B(1):212–7.
- [12] Williams CB, Cochran JK, Rosen DW. Additive manufacturing of metallic cellular materials via three-dimensional printing. *Int J Adv Manuf Technol* 2011;53(1–4):231–9.
- [13] Yeong WY, Chua CK, Leong KF, Chandrasekaran M. Rapid prototyping in tissue engineering: challenges and potential. *Trends Biotechnol* 2004;22(12):643–52.
- [14] Khalifa A, Vogt S, Weisser J, Grimm G, Rechtenbach A, Meyer W, et al. Development of a new calcium phosphate powder-binder system for the 3D printing of patient specific implants. *J Mater Sci Mater Med* 2007;18(5):909–16.
- [15] Peters F, Haenel T, Bernhardt A, Lode A, Gelinsky M, Duerr H. In vitro examination of 3D printed vs. milled scaffolds from beta-tricalcium phosphate (beta-TCP) for patient individual bone regeneration. 8th World Biomaterials Congress, Amsterdam; 2008.
- [16] Will J, Melcher R, Treul C, Travitky N, Kneser U, Polykandriotis E, et al. Porous ceramic bone scaffolds for vascularized bone tissue regeneration. *J Mater Sci – Mater Med* 2008;19(8):2781–90.
- [17] Leukers B, Gulkan H, Irsen SH, Milz S, Tille C, Schieker M, et al. Hydroxyapatite scaffolds for bone tissue engineering made by 3D printing. *J Mater Sci Mater Med* 2005;16(12):1121–4.
- [18] Karageorgiou V, Kaplan D. Porosity of 3D biomaterial scaffolds and osteogenesis. *Biomaterials* 2005;26(27):5474–91.
- [19] Vacanti JP, Cima LG, Cima MJ. Vascularized tissue regeneration matrices formed by solid free form fabrication techniques. U.S. Patent No. 6,176,874 B1; 2001.
- [20] Sachs E, Cima M, Williams P, Brancazio D, Cornie J. 3-Dimensional printing – rapid tooling and prototypes directly from a CAD model. *J Eng Ind – Trans ASME* 1992;114(4):481–8.
- [21] Holme I. Advances in the science and technology of paints, inks and related coatings. *Surf Coat Int Part B – Coat Trans* 2006;89(4):343–63.
- [22] Rane SB, Seth T, Phatak GJ, Amalnerkar DP, Das BK. Influence of surfactants treatment on silver powder and its thick films. *Mater Lett* 2003;57(20):3096–100.
- [23] Lin JC, Wang CY. Effects of surfactant treatment of silver powder on the rheology of its thick-film paste. *Mater Chem Phys* 1996;45(2):136–44.
- [24] Hogeckamp S, Pohl M. Methods for characterizing wetting and dispersing of powder. *Chem Ing Tech* 2004;76(4):385–90.
- [25] Lanzetta M, Sachs E. Improved surface finish in 3D printing using bimodal powder distribution. *Rapid Prototyping J* 2003;9(3):157–66.
- [26] Bohner M, Luginbuhl R, Reber C, Doebelin N, Baroud G, Conforto E. A physical approach to modify the hydraulic reactivity of alpha-tricalcium phosphate powder. *Acta Biomater* 2009;5(9):3524–35.
- [27] Spillmann A, Sonnenfeld A, Rudolf von Rohr P. Method for the attachment of nanoparticles to substrate particles. International Patent No. WO/2007/036060; 2007.
- [28] Spillmann A, Sonnenfeld A, von Rohr PR. Effect of surface free energy on the flowability of lactose powder treated by PECVD. *Plasma Process Polym* 2008;5(8):753–8.
- [29] Sonnenfeld A, Spillmann A, Arpagaus C, von Rohr PR. Application of plasma surface treatment to solid-state microscopic particulates. *Plasma Process Polym* 2009;6(3):170–9.
- [30] Spillmann A, Sonnenfeld A, von Rohr PR. Gravimetric and chemical characterization of SiO_x structures deposited on fine powders by short plasma exposure in a plasma down stream reactor. *Appl Surf Sci* 2008;255(5):1911–5.
- [31] Spillmann A. Flowability modification of lactose powder by plasma enhanced chemical vapor deposition. *Plasma Process Polym* 2007(4):S16–20.
- [32] Beamson G, Briggs D. High resolution XPS of organic polymers. Chichester: Wiley; 1992.
- [33] Shirley DA. High-resolution X-ray photoemission spectrum of valence bands of gold. *Phys Rev B* 1972;5(12):4709.
- [34] Rodriguez-Carvajal J. Recent developments of the program FULLPROF. Commission on powder diffraction (IUCr). Newsletter 2001;26:12–9.
- [35] Dickens B, Schroeder LW, Brown WE. Crystallographic studies on the role of Mg as a stabilizing impurity in β-Ca₃(PO₄)₂. I. The crystal structure of pure β-Ca₃(PO₄)₂. *J Solid State Chem* 1974;10:232–48.
- [36] Sudarsanan K, Young RA. Significant precision in crystal structure details: holly springs hydroxyapatite. *Acta Crystallogr* 1969;B25:1534–43.
- [37] Boudin S, Grandin A, Borel MM, Leclaire A, Raveau B. Redetermination of the β-Ca₂P₂O₇ structure. *Acta Crystallogr C* 1993;49(12):2062–4.
- [38] Mathew M, Schroeder LW, Dickens B, Brown WE. Crystal-structure of alpha-Ca₃(PO₄)₂. *Acta Crystallogr Sect B – Struct Sci* 1977;33(13):1325–33.
- [39] Langford JI, Wilson AJC. Scherrer after 60 years – survey and some new results in determination of crystallite size. *J Appl Crystallogr* 1978;11:102–13.
- [40] DIN EN 725-8. Advanced technical ceramics – methods of test for ceramic powders – part 8: determination of tapped bulk density; 2006. <http://www.beuth.de/langanzeige/DIN-EN-725-8/de/88828024.html&bcrumblelevel=4&SearchID=282576440>.
- [41] DIN EN 725-9. Advanced technical ceramics – methods of test for ceramic powders – part 9: determination of untapped bulk density; 2006. <http://www.beuth.de/langanzeige/DIN-EN-725-9/de/88827999.html&bcrumblelevel=3&SearchID=282577090>.
- [42] Schulze D, Wittmaier A. Flow properties of highly dispersed powders at very small consolidation stresses. *Chem Eng Technol* 2003;26(2):133–7.
- [43] Schulze D. Flowability of bulk solids – definition and measuring principles. *Chem Ing Tech* 1995;67(1):60–8.
- [44] Lazghab M, Saleh K, Pezron I, Guignon P, Komunjer L. Wettability assessment of finely divided solids. In: 4th French meeting on powder science and technology, Compiegne, France; 2004. p. 79–91.
- [45] Arpagaus C. Plasma surface modification of polymer powders in a downer reactor. Zurich: Swiss Federal Institute of Technology; 2005.
- [46] Washburn EW. The dynamics of capillary flow. *Phys Rev* 1921;17(3):273–83.
- [47] Grundke K, Boerner M, Jacobasch HJ. Characterization of fillers and fibers by wetting and electrokinetic measurements. *Colloids Surf* 1991;58(1–2):47–59.
- [48] Gbureck U, Hoelzel T, Biermann I, Barralet JE, Grover LM. Preparation of tricalcium phosphate/calcium pyrophosphate structures via rapid prototyping. *J Mater Sci – Mater Med* 2008;19(4):1559–63.
- [49] Melcher R. Rapid prototyping von Keramiken durch 3D-Drucken. PhD thesis. Erlangen, Germany: Universität Erlangen-Nürnberg; 2009.
- [50] Moulder JF, Stickle WF, Sobol PE, Bomben KD. Handbook of X-ray photoelectron spectroscopy. Eden Prairie, MN: Physical Electronics; 1995.
- [51] Korner L, Sonnenfeld A, Heuberger R, Waller JH, Leterrier Y, Manson JAE, et al. Oxygen permeation, mechanical and structural properties of multilayer diffusion barrier coatings on polypropylene. *J Phys D-Appl Phys* 2010;43(11).
- [52] Nebelung M, Lang B. Flowability of ceramic bulk materials part 2: interaction of primary particle properties and flowability. *CFI – Ceram For Int* 2009;86(4):E35–8.
- [53] Nebelung M, Lang B. Flowability of ceramic bulk materials part 1: methods. *CFI – Ceram For Int* 2009;86(3):E35–40.
- [54] Schulze D. Pulver und Schüttgüter, Fließigenschaften und Handhabung. Berlin/Heidelberg: Springer; 2009.
- [55] Roth C, Kuensch Z, Sonnenfeld A, von Rohr PR. Plasma surface modification of powders for pharmaceutical applications. *Surf Coat Technol* 2011;205:597–600.
- [56] Zimmermann I, Eber M, Meyer K. Nanomaterials as flow regulators in dry powders. *Z Phys Chem – Int J Res Phys Chem Chem Phys* 2004;218(1):51–102.
- [57] Kwade A, Schulze A, Schwedes J. Auslegung von Silos: Unmittelbare Messung des Horizontallastverhältnisses. *Beton-und Stahlbetonbau* 1994;89:58–63. 117–119.
- [58] ISO 6186. Plastics – determination of pourability. http://www.iso.org/iso/iso_catalogue/catalogue_tc/catalogue_detail.htm?csnumber=25202.
- [59] ISO 4324. Surface active agents – powders and granules – measurement of the angle of repose. http://www.iso.org/iso/iso_catalogue/catalogue_tc/catalogue_detail.htm?csnumber=10196.
- [60] Shanjani Y, Toyserkani E, Wei C. ASME. Modeling and characterization of biomaterials spreading properties in powder-based rapid prototyping techniques. In: ASME international mechanical engineering congress and exposition, Seattle, WA; 2007. p. 135–43.
- [61] Utela BR, Storti D, Anderson RL, Ganter M. Development process for custom three-dimensional printing (3DP) material systems. *J Manuf Sci Eng – Trans ASME* 2010;132(1):9.
- [62] Curodeau A, Sachs E, Caldarise S. Design and fabrication of cast orthopedic implants with freeform surface textures from 3-D printed ceramic shell. *J Biomed Mater Res* 2000;53(5):525–35.
- [63] Cima M, Sachs EM, Fan T, Bredt JF, Michaels SP, Khanuja S, et al. Three-Dimensional Printing Techniques. U.S. Patent No. 5,387,380; 1995.
- [64] Palzer S, Hiebl C, Sommer K, Lechner H. Influence of roughness of a solid surface on the angle of contact. *Chem Ing Tech* 2001;73(8):1032–8.

- [65] Spori DM, Drobek T, Zurcher S, Ochsner M, Sprecher C, Muehlebach A, et al. Beyond the lotus effect: Roughness, influences on wetting over a wide surface-energy range. *Langmuir* 2008;24(10):5411–7.
- [66] Fan T. Droplet-powder impact interaction in three dimensional printing. Cambridge, MA: Massachusetts Institute of Technology; 1995.
- [67] Sachs EEA. Three dimensional printing: the physics and implications of additive manufacturing. *CIRP Ann* 1993;42:257–60.
- [68] Camire CL, Nevsten P, Lidgren L, McCarthy I. The effect of crystallinity on strength development of alpha-TCP bone substitutes. *J Biomed Mater Res Part B* 2006;79B(1):159–65.
- [69] Igawa K, Mochizuki M, Sugimori O, Shimizu K, Yamazawa K, Kawaguchi H, et al. Tailor-made tricalcium phosphate bone implant directly fabricated by a three-dimensional ink-jet printer. *J Artif Organs* 2006;9(4):234–40.
- [70] Saijo H, Igawa K, Kanno Y, Mori Y, Kondo K, Shimizu K, et al. Maxillofacial reconstruction using custom-made artificial bones fabricated by inkjet printing technology. *J Artif Organs* 2009;12(3):200–5.
- [71] Seitz H, Deisinger U, Leukers B, Detsch R, Ziegler G. Different calcium phosphate granules for 3-D printing of bone tissue engineering scaffolds. *Adv Eng Mater* 2009;11(5):B41–6.
- [72] Sharif H, Shanjani Y, Vlasea M, Toyserkani E, ASME. On the bio-mechanical properties of a dual-porous osteochondral scaffold. In: ASME international mechanical engineering congress and exposition, Am Soc Mech Eng, Boston, MA; 2008. p. 17–24.
- [73] Shanjani Y, Toyserkani E. On mechanical properties of SFF-made calcium polyphosphate bio-structures. Boca Raton: CRC Press, Taylor & Francis Group; 2010.